

# Effects of substrate crystallographic orientations on crystal growth and microstructure development in laser surface-melted superalloy single crystals. Mathematical modeling of single-crystal growth in a melt pool (Part II)

Weiping Liu \*, J.N. DuPont

*Department of Materials Science and Engineering, Lehigh University, 5 E. Packer Avenue, Bethlehem, PA 18015, USA*

Received 25 February 2004; received in revised form 30 November 2004; accepted 3 December 2004

Available online 8 January 2005

## Abstract

The mathematical model developed for single-crystalline solidification in laser surface melting (LSM) described in Part I [Acta Mater 2004;52:4833–4847] was used to compute the dendrite growth pattern and velocity distribution in the 3D melt pool for various substrate orientations. LSM experiments with single-crystal nickel-base superalloys were conducted for different orientations to verify the computational results. Results show that the substrate orientation has a predominant effect on crystal growth pattern, and simultaneously influences the magnitude and distribution of dendrite growth velocity in the melt pool. The selected  $\langle 1\ 0\ 0 \rangle$  growth variants and the number of the chosen growth variants are dependent on the substrate orientation. The maximum velocity ratio (dendrite growth velocity over the beam velocity,  $V/V_b$ ) in the melt pool is a function of melt-pool geometrical parameters and the substrate orientation. The largest maximum velocity-ratio among the symmetric orientations is 1.414 for the  $(0\ 0\ 1)/[1\ 1\ 0]$  and  $(0\ 1\ 1)/[0\ 1\ \bar{1}]$  orientations, while that value for asymmetric orientations is 1.732 for the  $(0\ 1\ 1)/[1\ 1\ \bar{1}]$  orientation. Good agreement was obtained between the predicted and experimentally observed microstructures. The results are discussed with the susceptibility to stray grain formation as a function of substrate orientations and melt-pool geometrical parameters. These findings have some important implications for single-crystal surface processing.

© 2004 Acta Materialia Inc. Published by Elsevier Ltd. All rights reserved.

*Keywords:* Laser treatment; Nickel alloys; Microstructure; Modeling; Melt pool

## 1. Introduction

In Part I, a mathematical model was developed for the 3D melt-pool geometry and single-crystalline solidification in a melt pool [1]. The effects of melt-pool geometrical parameters on crystal growth pattern and velocity in the melt pool were studied computationally

using the model for laser surface melts along the  $[1\ 0\ 0]$  direction on the  $(0\ 0\ 1)$  plane of a single-crystal substrate. Under this condition, the maximum dendrite growth velocity during melt-pool solidification is equal to or less than the travel speed of the laser beam, depending on the melt-pool geometry. In this paper (Part II), the effect of substrate orientations on crystal growth direction and velocity in the melt pool is studied. Computations were conducted for laser melt-pools under eight specific crystallographic orientations of the substrate relative to laser scanning direction. Some of

\* Corresponding author. Tel.: +1 610 758 5943; fax: +1 610 758 6407.

E-mail address: [wel2@lehigh.edu](mailto:wel2@lehigh.edu) (W. Liu).

these crystallographic orientations are symmetric, and some others are asymmetric with respect to the melt-pool centerline. Calculation results are discussed regarding the susceptibility to stray grain formation as a function of melt-pool geometrical parameters and the substrate crystallographic orientation. Implications of the modeling results to practical applications in laser surface processing of single crystals are also presented. Laser surface processing of single-crystal alloys under various substrate-orientation conditions can be encountered in practical applications, such as the laser surface melting (LSM) or cladding of curved blades and vanes for repair.

Rappaz et al. [2,3] studied the microstructure development in full-penetration electron beam welds of Fe–15Ni–15Cr stainless steel single crystals for different weld orientations. They developed a relationship between the dendrite growth velocity and the welding velocity, and reconstructed the weld pool shape based on the observed dendritic structure to explain the microstructure developments in the welds of different orientations. However, in the work by Rappaz et al., the reconstructed weld pool was fixed in shape (i.e., invariable weld pool parameters). In this work, a new melt-pool model with four variable geometrical parameters is used in combination with the dendrite growth concepts to predict dendrite growth directions and velocities as a function of substrate orientation and melt-pool geometrical parameters. This approach allows direct determination of dendrite growth directions and velocities, and more importantly it enables a systematic study of the combined effect of substrate orientation and melt-pool geometry on the crystal growth in a laser surface melt pool.

## 2. Experimental procedure

LSM experiments were conducted on single-crystal nickel-base superalloys for various orientation conditions, using a Nd:YAG laser in the laser engineered net shaping (LENS) system to verify the model computation results. Two commercial nickel-base superalloy single crystals, designated, respectively, as Rene N5 alloy and CMSX-4 alloy, were used in the LSM experiments. The nominal composition of the N5 alloy is Ni–8Co–7Cr–6.2Al–5W–6Ta–3Re–2Mo–0.2Hf (in wt%) while the CMSX-4 alloy has a nominal composition of Ni–9Co–6.5Cr–5.6Al–1Ti–6W–6.5Ta–3Re–0.6Mo–0.1Hf (in wt%). The single crystals were obtained from Concorde Castings (Eastlake, OH) in plates for the N5 alloy and in bars for the CMSX-4 alloy. Due to the difficulty in obtaining specimens in a complicated orientation condition, only several representative orientations were chosen for the purpose of experimental verification. According to the crystal shapes and orientation, the

CMSX-4 alloy was used for LSM in the symmetric  $(0\ 0\ 1)/[1\ 1\ 0]$ <sup>1</sup> orientation, while the N5 alloy was used for LSM in the asymmetric  $(0\ 0\ 1)/[1\ 2\ 0]$  and  $(2\ 1\ 0)/[0\ 0\ 1]$  orientations (these orientations were chosen because specimens of enough size in these orientations can be cut according to the original crystal shape and orientation). The as-cast single crystals were carefully cut into specimens in the above orientations for LSM experiments. The substrate surfaces to be laser-melted were ground with 600-grit SiC paper and cleaned in methanol before LSM.

An Optomec LENS™ 750 system [1] was used for the LSM experiments. The Nd:YAG laser in this system has a circular beam with a Gaussian intensity distribution and a maximum output power of 750 W. The oxygen level in the Ar-gas atmosphere glove box was below 30 ppm during the LSM processing. The LENS system is equipped with a melt-pool sensor that provides a 2D infra-red image of the molten pool on the substrate surface. Experiments were conducted under different processing conditions by changing the laser power and travel velocity (Table 1). The melt-pool half-width ( $w$ ), depth ( $h$ ) and the  $\alpha$  angle were directly measured from the photomicrographs of the transverse cross-sections. The melt-pool length parameter ( $l$ ) was determined from the 2D video image of the melt pool or from direct measurements of the melt-pool traces (ripple formation) on the top surface of the melt track. Samples for microstructure analysis were mounted and polished using standard metallographic techniques and etched with a solution containing H<sub>2</sub>O (100 ml), HCl (100 ml) and CuCl<sub>2</sub> (5 g).

## 3. Results

### 3.1. $[1\ 1\ 0]$ laser scanning direction on $(0\ 0\ 1)$ plane

In this orientation, the  $x$ -,  $y$ - and  $z$ -axes are the  $[1\ 1\ 0]$ ,  $[\bar{1}\ 1\ 0]$  and  $[0\ 0\ 1]$  directions. Fig. 1 shows the computational results of dendrite growth direction and velocity on the melt-pool solidification interface for a melt pool of the geometrical parameters  $l/w = 1.5$ ,  $h/w = 1$  and  $\alpha = 90^\circ$  in this substrate orientation. From the dendrite growth pattern (Fig. 1(a)) plotted in the  $y$ - $z$  plane, three regions corresponding to three growth directions can be observed. In the bottom region of the melt pool, the  $[0\ 0\ 1]$  growth direction is favored. The  $[1\ 0\ 0]$  and  $[0\ 1\ 0]$  growth directions are chosen for the upper region of the melt pool in the  $+y$  side and in the  $-y$  side, respectively. At the upper part of the melt-pool centerline, the possibility of the dendrite to grow along either the  $[1\ 0\ 0]$

<sup>1</sup> Laser traveling along the  $[1\ 1\ 0]$  direction on the  $(0\ 0\ 1)$  plane, hereafter.

Table 1  
Laser processing parameters used in experiments and the measured melt pool geometry

Track no.	1	2	3	4	5
Material	CMSX-4	CMSX-4	CMSX-4	N5	N5
Orientation	(0 0 1)/[1 1 0]	(0 0 1)/[1 1 0]	(0 0 1)/[1 1 0]	(0 0 1)/[1 2 0]	(2 1 0)/[0 0 1]
Power (W)	200	200	475	285	285
Velocity (mm/s)	2.5	5	30	5	5
w (mm)	0.51	0.44	0.55	0.68	0.6
h (mm)	0.22	0.2	0.22	0.275	0.23
l (mm)	0.5	0.49	1.64	0.74	0.67
$\alpha$ (°)	78	78 (left) 54 (right)	88	90	90

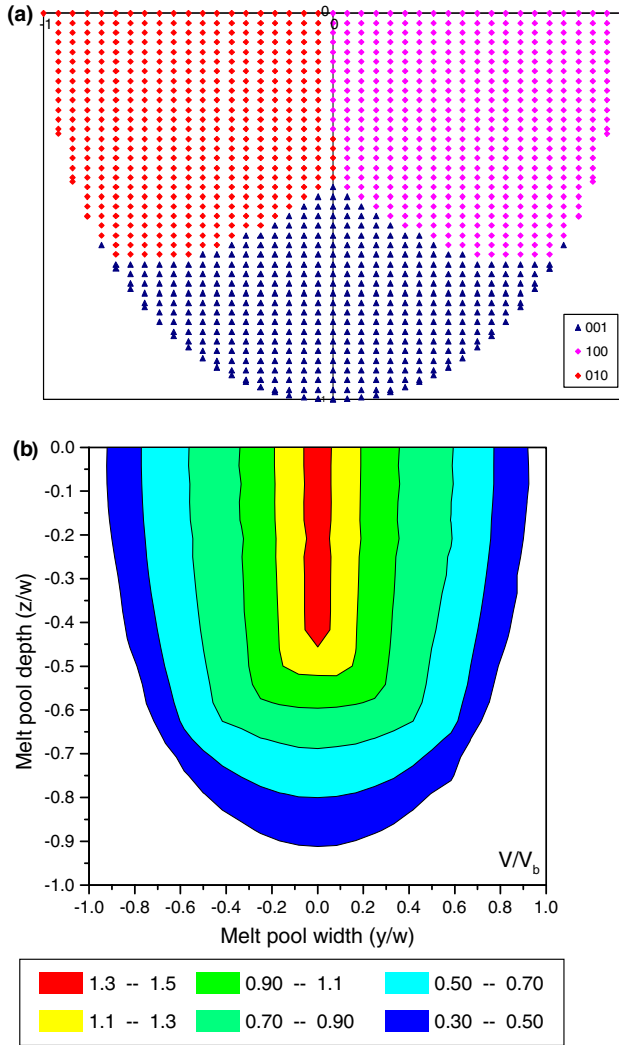


Fig. 1. Computed results of dendrite growth direction (a) and velocity ratio ( $V/V_b$ ) (b) in a melt pool of the geometrical parameters  $l/w = 1.5$ ,  $h/w = 1$  and  $\alpha = 90^\circ$  with the (0 0 1)/[1 1 0] orientation.

or [0 1 0] direction is the same since in each case the value of the angle  $\Psi$  is equal. As shown in Fig. 1(b), the dendrite growth velocity increases gradually from zero at the bottom and the sides of the melt pool to a maximum value ( $1.414V_b$ ) at the upper part of the centerline on the melt-pool interface, i.e. the boundary line between the

[1 0 0] and [0 1 0] growth regions. In this case, the maximum growth velocity is larger than the laser beam travel velocity. Fig. 2(a) shows the variation of dendrite growth velocity along the centerline on the melt-pool interface. The relative melt-pool depth ( $z/w$ ) along the centerline is also shown in this figure for reference. The beginning point of the maximum dendrite growth velocity ( $1.414V_b$ ) corresponds to the transition of dendrite growth direction from [0 0 1] to [1 0 0]/[0 1 0] at the centerline. At the transition point, the angle  $\theta$  equals to  $35.26^\circ$  ( $V/V_b = \cot \theta = 1.414$ ), and  $\psi_{001}$ ,  $\psi_{100}$  and  $\psi_{010}$  (the angles between the normal to the interface and [0 0 1], [1 0 0] and [0 1 0] directions, respectively) all have the same value, which is  $54.74^\circ$ . Fig. 2(b) shows the variation of dendrite growth velocity along the melt-pool trace line on the top surface, together with the variation of the relative melt-pool width ( $y/w$ ) on this surface. For symmetry reasons, the results in this figure are only for the [0 1 0] growth region, i.e. at the  $-y$  side. There is no transition of growth direction along the trace line on either side, and the [0 1 0] to [1 0 0] growth transition occurs exactly at the melt-pool centerline. The dendrite growth velocity increases gradually from zero at the sides of the melt pool to  $1.414V_b$  at the trailing point of the melt-pool.

Variations in the geometrical parameters ( $l/w$ ,  $h/w$ , and  $\alpha$ ) will change the relative areas of the [0 0 1], [1 0 0] and [0 1 0] growth regions. A smaller  $l/w$  ratio, a larger  $h/w$  ratio or a larger  $\alpha$  angle will promote the [1 0 0] and [0 1 0] dendrite growth by increasing the slope of the melt-pool interface. On the other hand, a larger  $l/w$  ratio, a smaller  $h/w$  ratio or a smaller  $\alpha$  angle will promote the [0 0 1] dendrite growth by decreasing the slope of the melt-pool interface. The relative area of the [0 0 1] growth region increases with an increase in the  $l/w$  value, a decrease in the  $h/w$  value or decrease in the  $\alpha$  value. As the [0 0 1] growth region increases, the triple point where the three growth regions meet at the melt-pool centerline moves upwards. When the triple point reaches the trailing (rearest) point of the melt pool, the following relationship exists:

$$\left(\frac{V_{001}}{V_b}\right)_{\max} = \tan \beta = \frac{w}{l} \cdot \tan \alpha = \sqrt{2}. \quad (1)$$

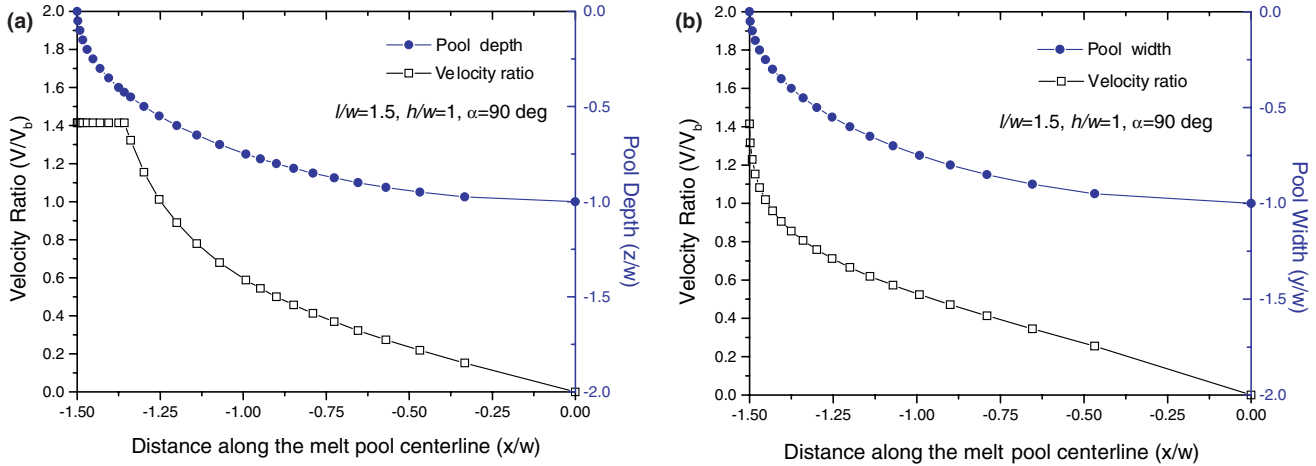


Fig. 2. (a) Variation of dendrite growth velocity ratio ( $V/V_b$ ) along the melt-pool boundary line in the  $x-z$  plane, together with the variation of the relative melt-pool depth on this line. (b) Variation of the velocity ratio ( $V/V_b$ ) along the melt-pool trace line in the  $x-y$  plane, together with the variation of the relative melt-pool width on this line. Melt-pool geometrical parameters:  $l/w = 1.5$ ,  $h/w = 1$  and  $\alpha = 90^\circ$ ; substrate orientation:  $(0\ 0\ 1)$   $[1\ 1\ 0]$ .

This is the critical condition for the disappearance of  $[1\ 0\ 0]$ / $[0\ 1\ 0]$  dendrite growth at the melt-pool centerline. Further increase in the  $[0\ 0\ 1]$  growth region leads to a maximum velocity ratio less than 1.414 in the melt-pool solidification, with a value as a function of  $l/w$  and  $\alpha$ . From Eq. (1), this occurs when  $\alpha$  is smaller than  $64.75^\circ$  for a  $l/w$  value of 1.5 or when  $l/w$  is larger than 2.64 for a  $\alpha$  value of  $75^\circ$ . It follows that under these conditions the maximum dendrite growth velocity in the melt-pool solidification can be controlled by changing the values of melt-pool geometrical parameters  $l/w$  and  $\alpha$ . As shown graphically in Fig. 3, the maximum velocity ratio under this orientation condition can be given as a function of melt-pool geometrical parameters ( $l/w$  and  $\alpha$ ) by the following equations:

$$\left(\frac{V}{V_b}\right)_{\max} = \frac{\tan \alpha}{l/w} \quad \left(\text{for } \frac{l}{w} \geq \frac{\sqrt{2}}{2} \tan \alpha\right), \quad (2)$$

$$\left(\frac{V}{V_b}\right)_{\max} = \sqrt{2} \quad \left(\text{for } \frac{l}{w} \leq \frac{\sqrt{2}}{2} \tan \alpha\right). \quad (3)$$

For an  $\alpha$  angle of  $90^\circ$  (no matter what value of the  $l/w$  ratio) or a  $l/w$  ratio less than  $0.7 \tan \alpha$ , the maximum velocity ratio is invariably 1.414. The maximum value of the  $V/V_b$  ratio decreases rapidly with decreasing  $\alpha$  value and increasing  $l/w$  ratio.

Fig. 4 shows the dendrite growth pattern and velocity results for a set of geometrical parameters  $l/w = 1.5$ ,  $h/w = 1$  and  $\alpha = 64^\circ$ . As can be seen, the decrease of  $\alpha$  angle from  $90^\circ$  to  $64^\circ$  significantly increases the relative area of the  $[0\ 0\ 1]$  growth region, and results in the disappearance of  $[1\ 0\ 0]$ / $[0\ 1\ 0]$  dendrite growth at the melt-pool centerline. The maximum value of the  $V/V_b$  ratio in this case is reduced to 1.36 (Fig. 4(b)). It is interesting to note that in Figs. 1(a) and 4(a) the transition lines between the  $[0\ 0\ 1]$  and  $[1\ 0\ 0]$  or  $[0\ 1\ 0]$  growth regions are of a non-symmetric parabola type in the  $y-z$  plane. With the decrease of  $\alpha$  angle, the non-symmetric parabola transition lines become narrower and move upwards, which reduces the relative areas of the  $[1\ 0\ 0]$  and  $[0\ 1\ 0]$  growth regions. When the  $\alpha$  angle is decreased to  $54.74^\circ$ , the transitions from  $[1\ 0\ 0]$  growth or  $[0\ 1\ 0]$  growth to  $[0\ 0\ 1]$  growth will occur at the side points of the melt pool in the  $y-z$  plane with coordinates of  $(0, w, 0)$  and  $(0, -w, 0)$ , respectively. This is demonstrated in Fig. 5(a) which shows the dendrite growth pattern for a set of geometrical parameters  $l/w = 1.5$ ,  $h/w = 0.5$  and  $\alpha = 54^\circ$ . Further computational results indicate that the  $[1\ 0\ 0]$  and  $[0\ 1\ 0]$  dendrite growths disappear completely when the  $\alpha$  angle is decreased to  $49^\circ$  for a

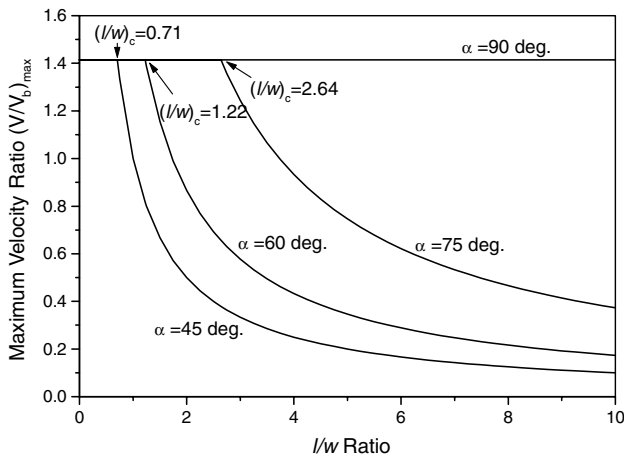


Fig. 3. Influence of  $\alpha$  values on the maximum velocity ratio as a function of the  $l/w$  ratio for the  $(0\ 0\ 1)$ / $[1\ 1\ 0]$  substrate orientation.

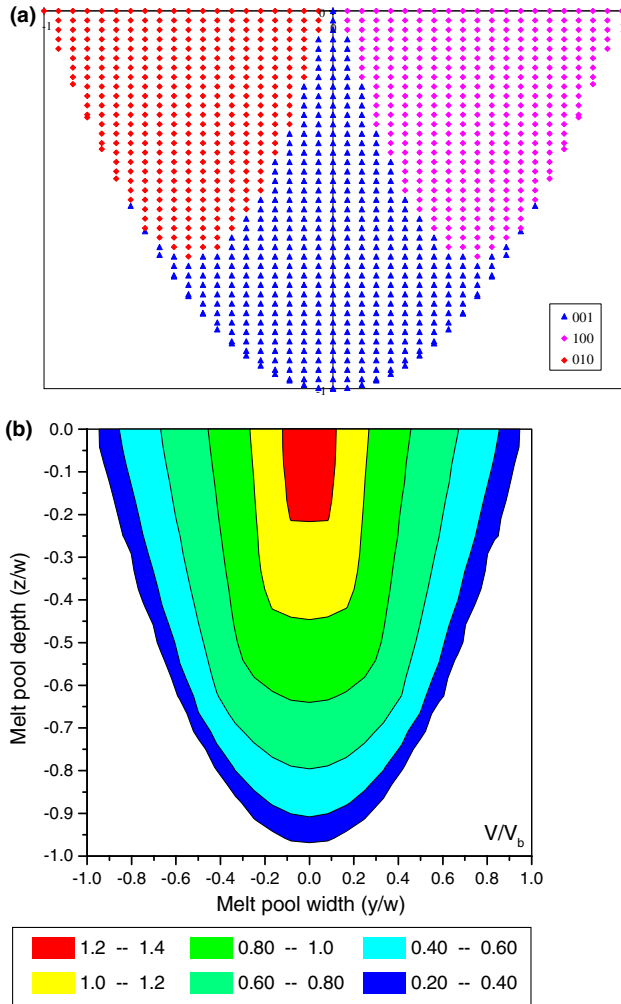


Fig. 4. Results of dendrite growth direction (a) and velocity ratio ( $V/V_b$ ) (b) in a melt pool of the geometrical parameters  $l/w = 1.5$ ,  $h/w = 1$  and  $\alpha = 64^\circ$  with the  $(0\ 0\ 1)/[1\ 1\ 0]$  orientation.

$l/w$  value of 1.5. As shown in Fig. 5(b), unidirectional dendrite growth along the  $[0\ 0\ 1]$  direction occurs in the melt pool. In this case, the maximum value of the  $V/V_b$  ratio for the melt-pool solidification is reduced to 0.76.

### 3.2. $[1\ 2\ 0]$ laser scanning direction on $(0\ 0\ 1)$ plane

This is a non-symmetric orientation with respect to the melt-pool centerline. In this orientation, the  $x$ -,  $y$ - and  $z$ -axes are the  $[1\ 2\ 0]$ ,  $[\bar{2}\ 1\ 0]$  and  $[0\ 0\ 1]$  directions. Fig. 6 shows the dendrite growth direction and velocity results for a melt pool of the geometrical parameters  $l/w = 1.5$ ,  $h/w = 1$  and  $\alpha = 90^\circ$  in this orientation. Four growth regions with a growth direction, respectively, of  $[0\ 0\ 1]$ ,  $[1\ 0\ 0]$ ,  $[\bar{1}\ 0\ 0]$  and  $[0\ 1\ 0]$  can be seen in the dendrite growth pattern (Fig. 6(a)) plotted in the  $y$ - $z$  plane. Unlike those discussed previously, the growth pattern is non-symmetric with respect to the melt-pool

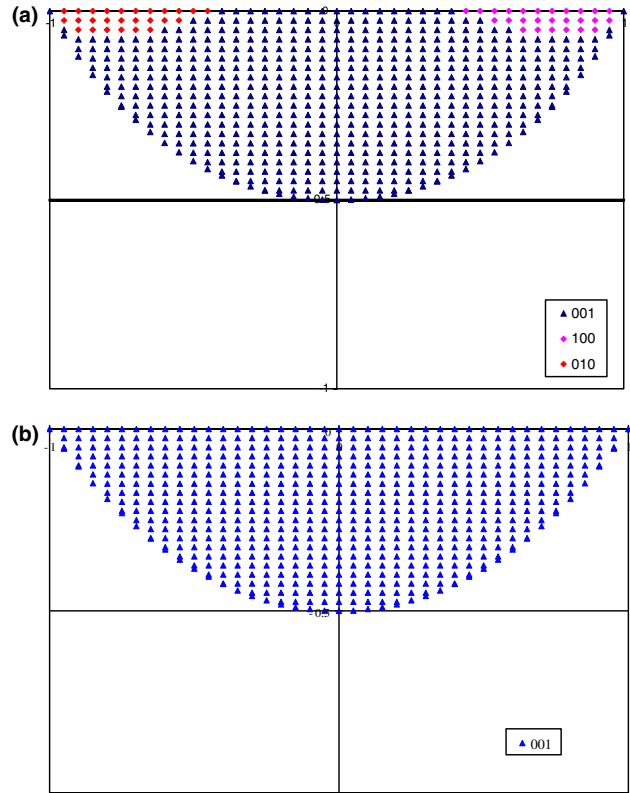


Fig. 5. Dendrite growth directions on the melt-pool solidification interface. Melt-pool geometrical parameters:  $l/w = 1.5$ ,  $h/w = 1$ ,  $\alpha = 54^\circ$  (a) and  $\alpha = 49^\circ$  (b); substrate orientation:  $(0\ 0\ 1)/[1\ 1\ 0]$ .

centerline due to the non-symmetry of the substrate orientation. As a result, the distribution of dendrite growth velocity is also asymmetric (Fig. 6(b)). Upon scrutiny of the velocity values, it is found that the location of the maximum velocity is away from the trailing point of the melt pool, at approximate coordinates of  $(-1.36w, 0.2w, -0.38w)$  in the  $x$ - $y$ - $z$  reference frame. This location corresponds to a transition of dendrite growth direction from  $[0\ 1\ 0]$  to  $[1\ 0\ 0]$ , as marked “M” in Fig. 6(a). The maximum velocity ratio in the melt pool for this orientation is 1.34.

### 3.3. $[1\ 0\ 0]$ laser scanning direction on $(0\ 1\ 1)$ plane

The  $x$ -,  $y$ - and  $z$ -axes are, respectively, in the  $[1\ 0\ 0]$ ,  $[0\ 1\ \bar{1}]$  and  $[0\ 1\ 1]$  directions for this substrate orientation. Fig. 7 shows the dendrite growth direction and velocity results for a melt pool in this orientation with a set of geometrical parameters  $l/w = 1.5$ ,  $h/w = 1$  and  $\alpha = 90^\circ$ . Only the  $[1\ 0\ 0]$ ,  $[0\ 1\ 0]$  and  $[0\ 0\ 1]$  growth regions exist in this case. In this orientation, the  $[0\ 0\ 1]$  and  $[0\ 1\ 0]$  directions are coplanar with the  $y$ - and  $z$ -axes and at an angle of  $45^\circ$  with the  $z$ -axis. The resulting growth pattern is therefore symmetric with respect to the melt-pool centerline. As shown in Fig. 7(a), the  $[1\ 0\ 0]$  growth region has an approximate shape of an

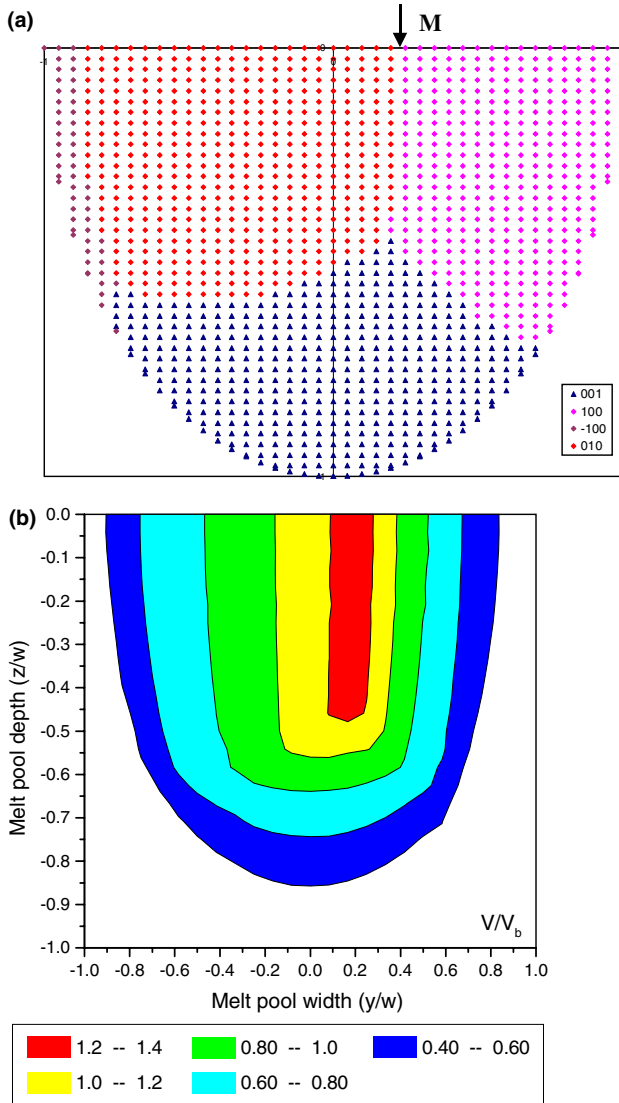


Fig. 6. Dendrite growth directions (a) and velocity ratios (b) on the melt-pool solidification interface. Melt-pool geometrical parameters:  $l/w = 1.5$ ,  $h/w = 1$  and  $\alpha = 90^\circ$ ; substrate orientation:  $(0\ 0\ 1)/[1\ 2\ 0]$ .

inversely placed triangle in the  $y$ - $z$  plane. Since the laser is travelling in the  $[1\ 0\ 0]$  direction, the dendrite growth velocity in the whole  $[1\ 0\ 0]$  growth region is equal to the travel velocity of the laser beam ( $V_b$ ), with a maximum velocity ratio being an unit in the melt pool in this orientation (Fig. 7(b)).

The size of the  $[1\ 0\ 0]$  growth region can be also controlled by changing the melt-pool geometrical parameters. According to Fig. 7(a), the  $[1\ 0\ 0]$  dendrite growth can be eliminated when the triple point moves to the trailing point of the melt pool. Under these critical conditions, the following relationships exist at the trailing point of the melt pool:

$$\cos \Psi_{1\ 0\ 0} = \cos \Psi_{0\ 0\ 1} = \cos \Psi_{0\ 1\ 0}, \quad (4)$$

$$\cos \Psi_{1\ 0\ 0} = \sin \beta, \quad (5)$$

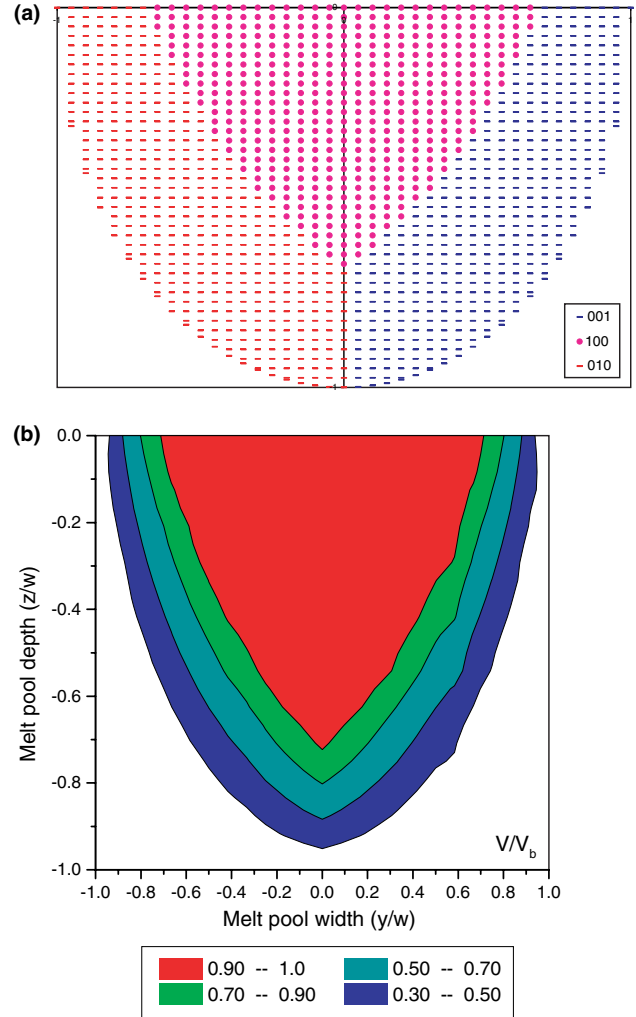


Fig. 7. Dendrite growth directions (a) and velocity ratios (b) on the melt-pool solidification interface. Melt-pool geometrical parameters:  $l/w = 1.5$ ,  $h/w = 1$  and  $\alpha = 90^\circ$ ; substrate orientation:  $(0\ 1\ 1)/[1\ 0\ 0]$ .

$$\cos \Psi_{0\ 0\ 1} = \cos \Psi_{0\ 1\ 0} = \frac{\sqrt{2}}{2} \cos \beta, \quad (6)$$

$$\tan \beta = \frac{\tan \alpha}{l/w}. \quad (7)$$

It can be derived from the above equations that no  $[1\ 0\ 0]$  dendrite growth exists in the melt pool when the  $\alpha$  angle is less than  $46.7^\circ$  for an  $l/w$  value of 1.5. Accordingly, the maximum velocity ratio in the melt pool in this orientation can be given as a function of melt-pool geometrical parameters ( $l/w$  and  $\alpha$ ) by the following equations:

$$\left(\frac{V}{V_b}\right)_{\max} = \frac{\sqrt{2} \tan \alpha}{l/w} \quad \left(\text{for } \frac{l}{w} \geq \sqrt{2} \tan \alpha\right), \quad (8)$$

$$\left(\frac{V}{V_b}\right)_{\max} = 1 \quad \left(\text{for } \frac{l}{w} \leq \sqrt{2} \tan \alpha\right). \quad (9)$$

### 3.4. $[0\ 1\ \bar{1}]$ laser scanning direction on $(0\ 1\ 1)$ plane

In this orientation, the  $x$ -,  $y$ - and  $z$ -axes are in the  $[0\ 1\ \bar{1}]$ ,  $[\bar{1}\ 0\ 0]$  and  $[0\ 1\ 1]$  directions, respectively. Fig. 8 shows the results of dendrite growth direction and velocity on the melt-pool solidification interface for the same set of geometrical parameters ( $l/w = 1.5$ ,  $h/w = 1$  and  $\alpha = 90^\circ$ ) in this substrate orientation. As shown in Fig. 8(a), the  $[1\ 0\ 0]$ ,  $[\bar{1}\ 0\ 0]$  and  $[0\ 1\ 0]$  growth regions exist in this case. A symmetric dendrite growth pattern is observed. In this orientation, the  $[\bar{1}\ 0\ 0]$  and  $[1\ 0\ 0]$  directions are parallel to the  $y$  and  $-y$  directions, respectively. Thus, the  $[\bar{1}\ 0\ 0]$  and  $[1\ 0\ 0]$  growth regions exist in the sides of the melt pool. The  $[0\ 1\ 0]$  and  $[0\ 0\ 1]$  directions are coplanar with the  $x$ - and  $z$ -axes and at an angle of  $45^\circ$  and  $135^\circ$  with the  $x$ -axis, respectively. The  $[0\ 1\ 0]$  growth direction is favored in the central part of the melt pool throughout the melt-pool depth. The distribution of dendrite growth velocities (Fig. 8(b)) is

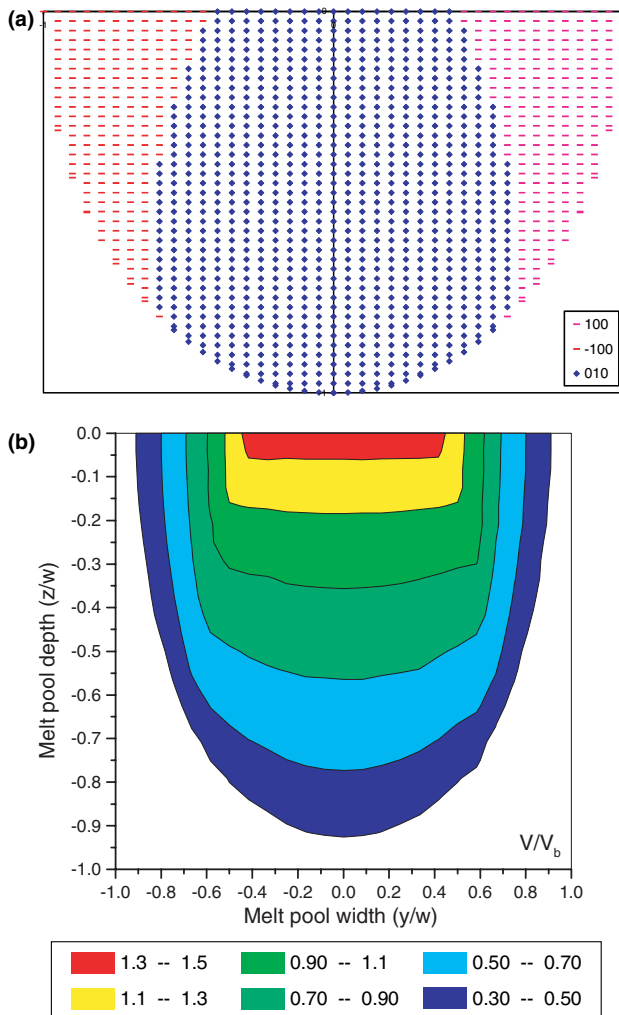


Fig. 8. Dendrite growth directions (a) and velocity ratios (b) on the melt-pool solidification interface. Melt-pool geometrical parameters:  $l/w = 1.5$ ,  $h/w = 1$  and  $\alpha = 90^\circ$ ; substrate orientation:  $(0\ 1\ 1)/[0\ 1\ \bar{1}]$ .

quite different from that observed in Fig. 7(b). In this case, the growth velocity increases continuously from the bottom and the sides to the rear part of the melt pool, with approximately rectangular contour lines in the regions of high growth velocities. The maximum velocity ratio is at the trailing point of the melt pool, located in the  $[0\ 1\ 0]$  growth region, which can be given by the following equation:

$$\left(\frac{V}{V_b}\right)_{\max} = \frac{\cos(90^\circ - \beta)}{\cos(\beta - 45^\circ)} = \frac{\sqrt{2}}{1 + \cot \beta} \quad (10)$$

Inserting Eq. (7) into Eq. (10), one can further obtain the relationship between the maximum velocity ratio and the melt-pool geometrical parameters

$$\left(\frac{V}{V_b}\right)_{\max} = \frac{\sqrt{2}}{1 + \cot \left[ \arctan \left( \frac{\tan \alpha}{l/w} \right) \right]} \quad (11)$$

For  $\alpha = 90^\circ$ , the maximum velocity ratio in the melt pool has the highest value of 1.414.

### 3.5. $[1\ 1\ \bar{1}]$ laser scanning direction on $(0\ 1\ 1)$ plane

In this case, the  $x$ -,  $y$ - and  $z$ -axes are in the  $[1\ 1\ \bar{1}]$ ,  $[\bar{2}\ 1\ \bar{1}]$  and  $[0\ 1\ 1]$  directions, respectively. Therefore, this is a non-symmetric orientation with respect to the melt-pool centerline. Fig. 9 shows the results of dendrite growth direction and velocity in the melt pool in this orientation with geometrical parameters  $l/w = 1.5$ ,  $h/w = 1$  and  $\alpha = 90^\circ$ . An asymmetric growth pattern can be seen in Fig. 9(a) due to the non-symmetry of this substrate orientation. Four growth regions exist in the melt pool, with the two major regions in the  $[1\ 0\ 0]$  and  $[0\ 1\ 0]$  growth directions, respectively, and the two minor regions in the  $[0\ 0\ 1]$  and  $[\bar{1}\ 0\ 0]$  growth directions, respectively. As shown in Fig. 9(b), the distribution of dendrite growth velocity is also non-symmetric with respect to the melt-pool centerline. The growth velocity increases continuously from the bottom and the sides to the rear part of the melt pool, with oblique triangular contour lines in the regions of high growth velocities. In spite of the non-symmetric velocity distribution, the maximum velocity ratio is located at the trailing point of the melt pool (Fig. 9(b)). Its value can be given by the following equation:

$$\left(\frac{V}{V_b}\right)_{\max} = \frac{\cos(90^\circ - \beta)}{\frac{\sqrt{3}}{3} \sin \beta + \frac{\sqrt{2}}{2} \cos \beta} = \frac{1}{\frac{\sqrt{3}}{3} + \frac{\sqrt{2}}{2} \cot \beta} \quad (12)$$

By inserting Eq. (7) into Eq. (12), the relationship between the maximum velocity ratio and the melt-pool geometrical parameters in this orientation can be expressed as

$$\left(\frac{V}{V_b}\right)_{\max} = \frac{1}{\frac{\sqrt{3}}{3} + \frac{\sqrt{2}}{2} \cot \left[ \arctan \left( \frac{\tan \alpha}{l/w} \right) \right]} \quad (13)$$

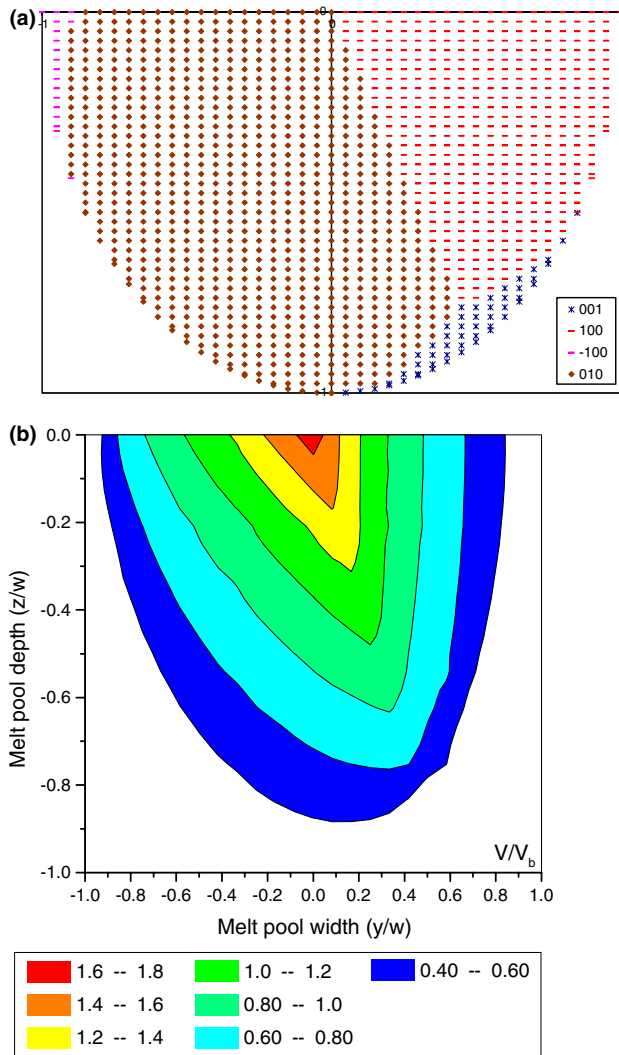


Fig. 9. Dendrite growth directions (a) and velocity ratios (b) on the melt-pool solidification interface. Melt-pool geometrical parameters:  $l/w = 1.5$ ,  $h/w = 1$  and  $\alpha = 90^\circ$ ; substrate orientation:  $(0\ 1\ 1)/[1\ 1\ 1]$ .

It should be pointed out that Eqs. (12) and (13) are only valid under the condition that the maximum velocity ratio is located at the trailing point of the melt pool. According to Eq. (13), for  $\alpha = 90^\circ$  the maximum velocity ratio in the melt pool has the highest value of 1.732 in this orientation. This value is also the largest that can be obtained in any substrate orientation.

3.6.  $[2\ \bar{1}\ 1]$  laser scanning direction on  $(0\ 1\ 1)$  plane

In this orientation, the  $x$ -,  $y$ - and  $z$ -axes are in the  $[2\ \bar{1}\ 1]$ ,  $[1\ 1\ \bar{1}]$  and  $[0\ 1\ 1]$  directions, respectively. This is also a non-symmetric orientation with respect to the melt-pool centerline. Fig. 10 shows the dendrite growth direction and velocity results for a melt pool in this orientation with geometrical parameters  $l/w = 1.5$ ,  $h/w = 1$  and  $\alpha = 90^\circ$ . Three growth regions with a growth direc-

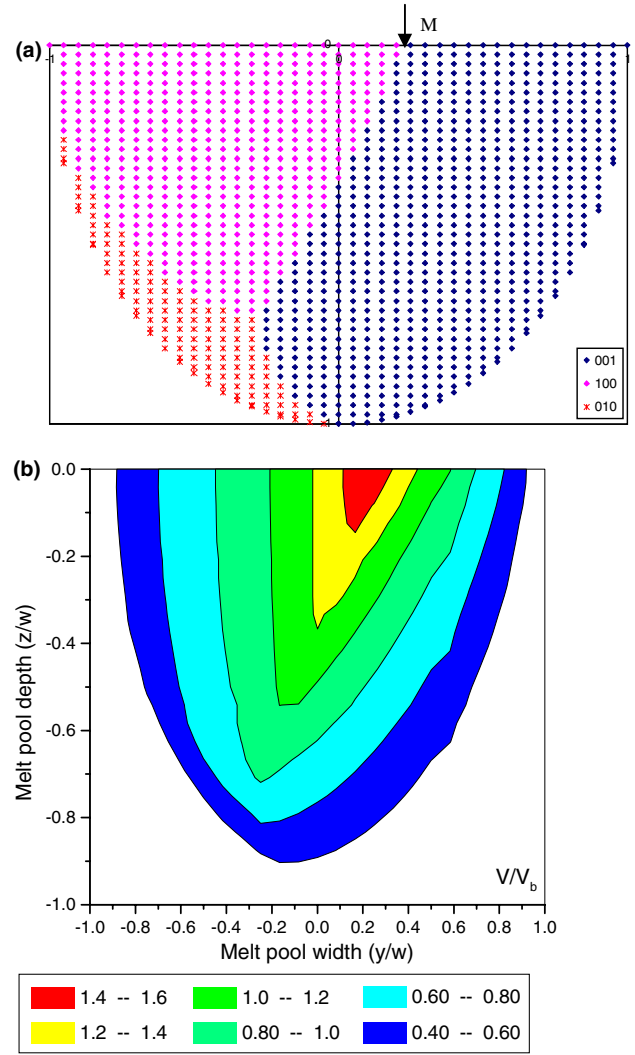


Fig. 10. Dendrite growth directions (a) and velocity ratios (b) on the melt-pool solidification interface. Melt-pool geometrical parameters:  $l/w = 1.5$ ,  $h/w = 1$  and  $\alpha = 90^\circ$ ; substrate orientation:  $(1\ 1\ 1)/[2\ \bar{1}\ 1]$ .

tion of  $[0\ 0\ 1]$ ,  $[1\ 0\ 0]$  and  $[0\ 1\ 0]$ , respectively, can be seen in the dendrite growth pattern (Fig. 10(a)) plotted in the  $y$ - $z$  plane. As a result of asymmetry of the substrate orientation, the growth pattern is non-symmetrical with respect to the melt-pool centerline. As shown in Fig. 10(b), the growth velocity increases also continuously from the bottom and both sides to the rear part of the melt pool, but the gradient in growth velocity in the  $[0\ 0\ 1]$  growth region is significantly higher than that in the  $[1\ 0\ 0]$  growth region. It is interesting to note that the maximum velocity is not located at the trailing point of the melt pool in this orientation. For the set of geometrical parameters used in this computation, the maximum velocity is located at approximate coordinates of  $(-1.46w, 0.23w, 0)$  in the  $x$ - $y$ - $z$  reference frame. This location also corresponds to a transition point of dendrite growth direction from  $[1\ 0\ 0]$  to  $[0\ 0\ 1]$  on the melt-pool surface, as marked “M” in Fig. 10(a). The

maximum velocity ratio in the melt pool is computed to be 1.63 for this orientation.

### 3.7. $[0\ 1\ \bar{1}]$ laser scanning direction on $(1\ 1\ 1)$ plane

In this case, the  $x$ -,  $y$ - and  $z$ -axes are in the  $[0\ 1\ \bar{1}]$ ,  $[\bar{2}\ 1\ 1]$  and  $[1\ 1\ 1]$  directions, respectively. This is again a non-symmetric orientation with respect to the melt-pool centerline. Fig. 11 shows the results of dendrite growth direction and velocity in the melt pool in this orientation with geometrical parameters  $l/w = 1.5$ ,  $h/w = 1$  and  $\alpha = 90^\circ$ . In the dendrite growth pattern shown in Fig. 11(a), there exist four growth regions with the  $[0\ 1\ 0]$ ,  $[1\ 0\ 0]$ ,  $[\bar{1}\ 0\ 0]$  and  $[0\ 0\ \bar{1}]$  growth directions, respectively. The  $[0\ 1\ 0]$  and  $[1\ 0\ 0]$  growth regions are the predominant ones in the melt pool in this orientation. The distribution of dendrite growth velocity in the melt pool, as shown in Fig. 11(b), is extremely asym-

metrical with respect to the melt-pool centerline. The gradient in growth velocity in the  $[1\ 0\ 0]$  growth region is much higher than that in the  $[0\ 1\ 0]$  growth region, as evidenced by the higher density of contour lines in the  $[1\ 0\ 0]$  region. Despite the extreme asymmetry observed in the velocity distribution, the maximum velocity ratio is located at the trailing point of the melt pool. Its value can be given by the following equations:

$$\left(\frac{V}{V_b}\right)_{\max} = \frac{\cos(90^\circ - \beta)}{\frac{\sqrt{2}}{2} \sin \beta + \frac{\sqrt{3}}{3} \cos \beta} = \frac{1}{\frac{\sqrt{2}}{2} + \frac{\sqrt{3}}{3} \cot \beta}, \quad (14)$$

$$\left(\frac{V}{V_b}\right)_{\max} = \frac{1}{\frac{\sqrt{2}}{2} + \frac{\sqrt{3}}{3} \cot \left[ \arctan \left( \frac{\tan \alpha}{l/w} \right) \right]}. \quad (15)$$

Again, Eqs. (14) and (15) apply only on the condition that the maximum velocity ratio is located at the trailing point of the melt pool. For  $\alpha = 90^\circ$ , according to Eq. (15), the maximum velocity ratio in the melt pool has the highest value of 1.414 in this orientation.

### 3.8. $[2\ \bar{1}\ \bar{1}]$ laser scanning direction on $(1\ 1\ 1)$ plane

The  $x$ -,  $y$ - and  $z$ -axes are in the  $[2\ \bar{1}\ \bar{1}]$ ,  $[0\ 1\ \bar{1}]$  and  $[1\ 1\ 1]$  directions in this orientation, respectively. According to crystallography in the cubic system, this orientation is symmetrical with respect to the melt-pool centerline. Fig. 12 shows the dendrite growth direction and velocity results for a melt pool in this orientation with geometrical parameters  $l/w = 1.5$ ,  $h/w = 1$  and  $\alpha = 90^\circ$ . The symmetrical substrate orientation leads to a symmetrical dendrite growth pattern, as indicated in Fig. 12(a). As many as five dendrite growth regions exist in the melt pool in this case with the  $[1\ 0\ 0]$ ,  $[0\ 0\ \bar{1}]$ ,  $[0\ 1\ 0]$  and  $[0\ \bar{1}\ 0]$  growth directions, respectively. The  $[1\ 0\ 0]$  growth region that is located in the central part of the melt pool is the largest one in the five regions. Among the six  $\langle 1\ 0\ 0 \rangle$  variants, five growth directions have been chosen in the melt-pool solidification in this orientation, which is the most that can be achieved in any substrate orientation. As shown in Fig. 12(b), the distribution of dendrite growth velocity in the melt pool is symmetrical with respect to the melt-pool centerline. The dendrite growth velocity increases much more rapidly from both sides than from the bottom to the rear part of the melt pool. The maximum velocity ratio is at the trailing point of the melt pool, located in the  $[1\ 0\ 0]$  growth region, which is given by the following equations:

$$\left(\frac{V}{V_b}\right)_{\max} = \frac{\cos(90^\circ - \beta)}{\frac{\sqrt{3}}{3} \cos \beta + \sqrt{\frac{2}{3}} \sin \beta} = \frac{1}{\sqrt{\frac{2}{3}} + \frac{\sqrt{3}}{3} \cot \beta}, \quad (16)$$

$$\left(\frac{V}{V_b}\right)_{\max} = \frac{1}{\sqrt{\frac{2}{3}} + \frac{\sqrt{3}}{3} \cot \left[ \arctan \left( \frac{\tan \alpha}{l/w} \right) \right]}. \quad (17)$$

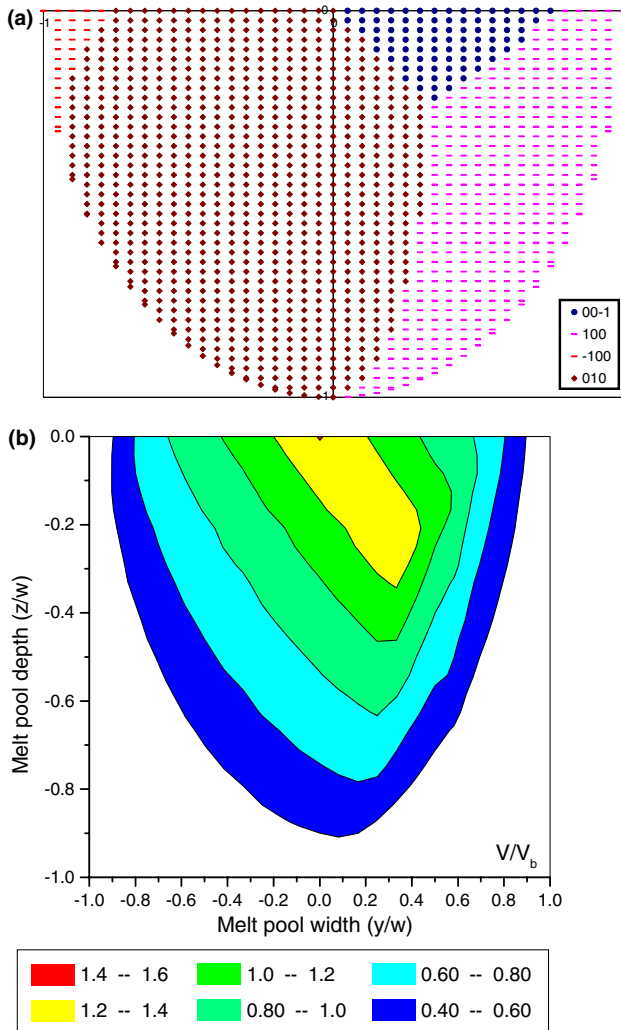


Fig. 11. Dendrite growth directions (a) and velocity ratios (b) on the melt-pool solidification interface. Melt-pool geometrical parameters:  $l/w = 1.5$ ,  $h/w = 1$  and  $\alpha = 90^\circ$ ; substrate orientation:  $(1\ 1\ 1)/[0\ 1\ \bar{1}]$ .

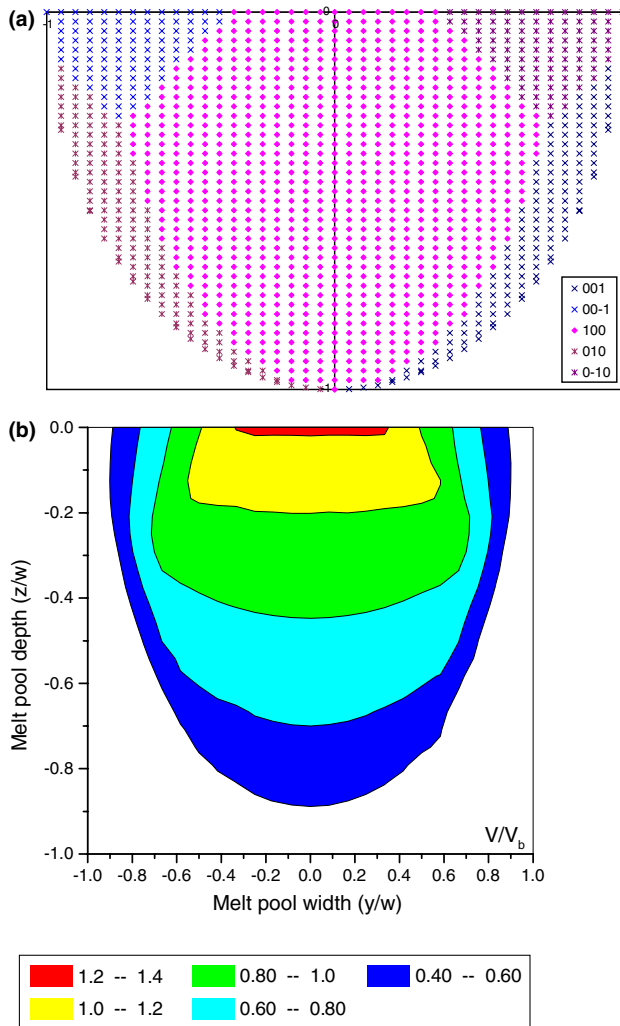


Fig. 12. Dendrite growth directions (a) and velocity ratios (b) on the melt-pool solidification interface. Melt-pool geometrical parameters:  $l/w = 1.5$ ,  $h/w = 1$  and  $\alpha = 90^\circ$ ; substrate orientation:  $(1\ 1\ 1)/[2\ \bar{1}\ \bar{1}]$ .

Since the maximum dendrite growth velocity is invariably located at the trailing point of the melt pool, Eq. (17) represents the relationship between the maximum velocity ratio and the melt-pool geometrical parameters in this orientation. For  $\alpha = 90^\circ$ , according to Eq. (17), the maximum velocity ratio in the melt pool has the largest value of 1.225 in this orientation.

### 3.9. Experimental verification

Fig. 13 shows the transverse-section microstructures of melt-tracks processed at different parameters in the  $(0\ 0\ 1)/[1\ 1\ 0]$  orientation and their comparisons with the computed microstructure patterns. In Fig. 13(a), the microstructure was obtained at a laser power of 200 W and a beam velocity of 2.5 mm/s, and the observed melt pool had a circular shape in the top surface. As can be seen, the cell-like dendrites grew in the  $[0\ 0\ 1]$  direction at the bottom of the melt pool, while the den-

drates at the upper regions grew in the  $[0\ 1\ 0]$  and  $[1\ 0\ 0]$  directions, respectively for the left and right sides, at an angle of  $45^\circ$  towards the outside of paper. The  $[0\ 1\ 0]$  and  $[1\ 0\ 0]$  dendrites impinged each other at the centerline of the melt pool. The observed microstructure agrees well with the computed microstructure pattern. As discussed in the companion paper (Part I) [1], the inaccuracy of substrate orientation brought by specimen preparation, some irregularities in the melt-pool boundary and slight discrepancy of the actual melt-pool shape from the exact mathematical formulation account for the small disagreement between the experimental observations and model predictions.

The observed microstructure shown in Fig. 13(b) is somehow significantly non-symmetrical, as is indicated by the big difference in the measured values of the  $\alpha$ -angle at both sides ( $78^\circ$  at the left side, and  $54^\circ$  at the right side). The non-symmetry of the melt-pool geometry can be caused by different heat and fluid flow conditions in the melt pool at the two sides, resulting from such factors as different surface tensions [4]. It is interesting that at the corner of the melt pool at the right side, as shown in Fig. 13(b), an essentially unidirectional dendrite growth in the  $[0\ 0\ 1]$  direction was observed due to a much smaller  $\alpha$ -angle. This experimental observation provides an effective verification for the model prediction that unidirectional dendrite growth along the  $[0\ 0\ 1]$  crystallographic direction can be achieved in the single-crystalline melt-pool solidification at an  $\alpha$ -angle below the critical value in a specific orientation. Using the same melt-pool width ( $w$ ), length ( $l$ ) and thickness ( $h$ ) and different  $\alpha$ -angle values for the two sides, the computed non-symmetric microstructure pattern agreed reasonably well with the observed microstructure. The size of unidirectional-growth zone from the model prediction is smaller than the observed one. This discrepancy could result from the use of the same values for other geometrical parameters and the local disagreement in the melt-pool shape at the corner for the asymmetrical situation.

In Fig. 13(c), the microstructure was made at a high beam velocity of 30 mm/s. In this case, the melt pool was significantly elongated in the beam traveling direction. Due to this change in melt-pool geometry, the  $[0\ 0\ 1]$  dendrites can grow almost up to the top at the melt-pool centerline. As shown in Fig. 13(c), the observed microstructure matched very well with the model prediction. Solidification cracking was observed in the melt track made at a high processing velocity, as is discussed in Part I [1].

Fig. 14(a) and (b) shows the transverse-section microstructures of melt-tracks processed, respectively, in the non-symmetrical  $(0\ 0\ 1)/[1\ 2\ 0]$  and  $(2\ 1\ 0)/[0\ 0\ 1]$  orientations and their comparisons with the computed microstructure patterns. In the melt track made in the  $(0\ 0\ 1)/[1\ 2\ 0]$  orientation, the cell-like dendrites grew in the

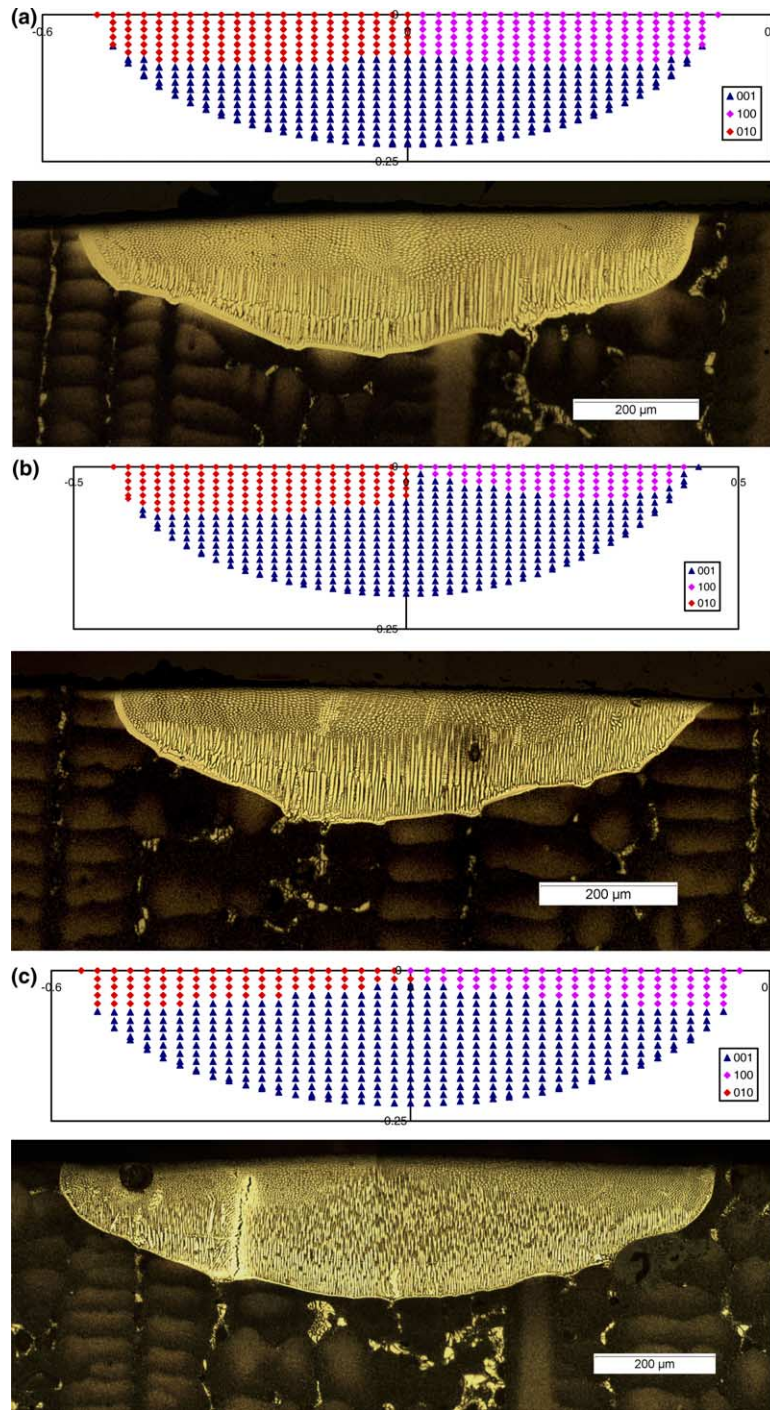


Fig. 13. Transverse-section microstructures of melt-tracks processed in the (0 0 1)/[1 1 0] orientation and their comparisons with the computed microstructure patterns. (a)  $P = 200$  W,  $V_b = 2.5$  mm/s; (b)  $P = 200$  W,  $V_b = 5$  mm/s; (c)  $P = 475$  W,  $V_b = 30$  mm/s.

[0 0 1] direction at the bottom of the melt pool, while the dendrites at the upper regions grew in the [0 1 0], [1 0 0] and  $[\bar{1} 0 0]$  directions, respectively. As can be seen, both the observed crystal growth regions and their relative sizes agreed well with the computed microstructure pattern in this orientation. In the microstructure obtained in the (2 1 0)/[0 0 1] orientation (Fig. 14(b)), the dendrites grew in the [1 0 0] direction (at an angle of about

$63^\circ$  with the  $y$ -axis in the section plane) at the bottom of the melt pool, while the dendrites at the upper regions grew in the  $[0 \bar{1} 0]$ , [0 0 1] and [0 1 0] directions, respectively, from the left to the right side. The computed microstructure patterns agreed reasonably well with the experimentally observed microstructure, although, some discrepancies were found between the computed and observed sizes of growth regions in this

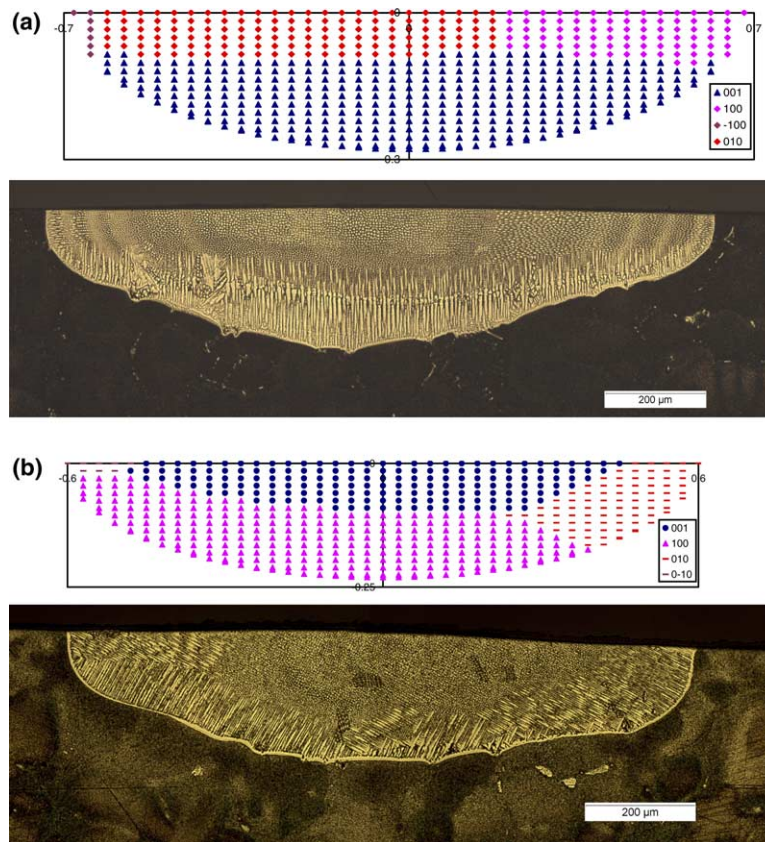


Fig. 14. Transverse-section microstructures of melt-tracks processed in (a)  $(0\ 0\ 1)/[1\ 2\ 0]$  and (b)  $(2\ 1\ 0)/[0\ 0\ 1]$  orientations and their comparisons with the computed microstructure patterns ( $P = 285\ \text{W}$ ,  $V_b = 5\ \text{mm/s}$ ). (Note: plotting symbols do not necessarily represent actual directions.)

microstructure. These discrepancies could result from the inaccuracy of substrate orientation and the local disagreement between an actual 3D melt-pool shape and the mathematical model.

#### 4. Discussion

The computational results of dendrite growth direction and velocity in the melt pool under the above eight orientation conditions have shown that the substrate crystallographic orientation has considerable effect on crystal growth direction and also influences the dendrite growth velocity in the single-crystalline melt-pool solidification. The selected  $\langle 1\ 0\ 0 \rangle$  growth variants, the number of the chosen growth variants, and growth velocities during the melt-pool solidification are all dependent on the substrate crystallographic orientation. The resulting microstructure (dendrite growth pattern) is obviously different from one substrate orientation to another. The magnitude and distribution of the dendrite growth velocity in the melt pool also vary from one case to another. These findings not only help to better understand the single-crystalline solidification behavior in a melt pool and predict the microstructure development (den-

drite growth pattern) computationally, but also can provide some implications to practical applications in single-crystal and polycrystalline materials processing.

One major problem encountered in welding and laser surface processing of single-crystal alloys is the loss of the single-crystal nature after processing, which is caused by the formation of equiaxed grains due to nucleation and growth of grains in the liquid ahead of the epitaxial columnar-dendritic solidification front. These equiaxed grains are also referred to as stray grains in the literature [5,6]. Recent research has shown that the formation of stray grains is related to the extent of constitutional supercooling ahead of the solidification interface [6,7]. In order to retain the single-crystal nature of the processed material for the purpose of desired properties, the nucleation of randomly oriented stray grains must be prevented. According to solidification theories [8,9], the constitutional supercooling (CS) criterion defines the conditions at which a planar solid-liquid interface breaks down and produces substructure (i.e., cells). The CS criterion can be expressed as

$$G/V < \Delta T_0/D, \quad (18)$$

where  $G$  is the temperature gradient in the liquid at the solidification interface,  $V$  is the growth velocity at the

solidification interface,  $\Delta T_0$  is the equilibrium solidification temperature range of the alloy, and  $D$  is the liquid diffusivity of the alloy. Although, this criterion does not explicitly define the extent of undercooling required to form equiaxed stray grains, recent work [6] has shown that the extent of CS can be used as an indication of the propensity for stray grain formation. For a particular material ( $\Delta T_0$  and  $D$  are fixed), Eq. (18) states that the  $G/V$  ratio is less than a constant. At a given temperature gradient, a larger dendrite growth velocity leads to a smaller  $G/V$  ratio, which increases the extent of CS and tends to enhance the propensity for stray grain formation. Conversely, a smaller dendrite growth velocity may give rise to a  $G/V$  ratio larger than the critical value to avoid the formation of equiaxed stray grains. The computational results of dendrite growth velocity in the melt pool indicate that the maximum velocity is located at (or close to for some cases of asymmetric substrate orientations) the trailing point of the melt pool, which explains the observed experimental phenomena that stray grains are usually present at the top region near the centerline in the laser-melted tracks. Similar experimental observations were made previously by David et al. [5] and Vitek et al. [6] in welds of single-crystal superalloys.

The temperature field and the corresponding temperature gradient ( $G_n$ ) in the normal direction of the melt-pool interface, which are determined by the processing conditions, are generally independent on the crystallographic orientation of the substrate material since the thermal properties of an alloy are usually isotropic. The temperature gradient ( $G$ ) along the dendrite growing direction  $[h k l]$  is given by

$$G = G_n \cdot \cos \Psi, \quad (19)$$

where  $\Psi$  is the angle between the normal ( $\vec{n}$ ) to the melt-pool interface and the  $[h k l]$  direction. The dendrite growth velocity in the melt pool, as shown in the previous sections, depends not only on the processing conditions, but on the crystallographic orientation of the substrate material as well. It follows that different substrate orientations give rise to different  $G/V$  values in the same location in the melt pool under the same processing conditions. Considering the trailing point in the melt pool, where the normal temperature gradient is generally lower and the growth velocity is the largest for symmetric orientations, the velocity ratio ( $V/V_b$ ) and the temperature gradient ratio ( $G/G_n$ ) are a function of the  $\beta$  angle. Fig. 15(a) and (b), respectively, show comparisons of the velocity ratio ( $V/V_b$ ) and the temperature gradient ratio ( $G/G_n$ ) at this trailing point in the melt pool as a function of the angle  $\beta$  for five different symmetrical substrate orientations. From Fig. 15(a) and (b), the value  $(G \cdot V_b)/(G_n \cdot V)$  that is proportional to  $G/V$  can be obtained also as a function of the  $\beta$  angle, as shown in Fig. 15(c), for different orientations. As

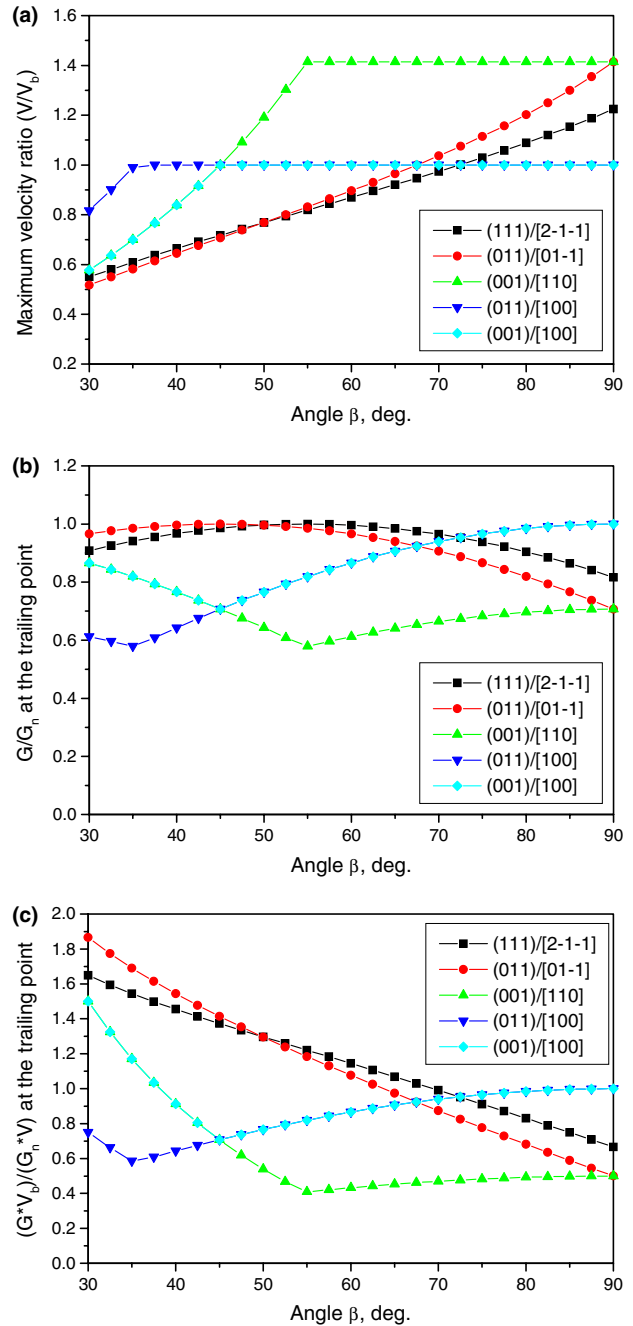


Fig. 15. Comparisons of (a) the velocity ratio ( $V/V_b$ ), (b) the temperature gradient ratio ( $G/G_n$ ) and (c) the value  $(G \cdot V_b)/(G_n \cdot V)$  at the trailing point in the melt pool as a function of the angle  $\beta$  for five different symmetrical substrate orientations.

mentioned before, the angle  $\beta$  is determined by the melt-pool geometrical parameters  $l/w$  and  $\alpha$  through Eq. (7). Based on Eq. (18), the smaller the value  $(G \cdot V_b)/(G_n \cdot V)$  in the melt pool for a specific substrate orientation (where  $V_b$  and  $G_n$  are values independent on orientation), the higher the propensity for stray grain formation. Among the five orientations, according to Fig. 15, the (0 0 1)/[1 0 0] and (0 1 1)/[1 0 0] orientations

are the most favorable ones for preventing the formation of stray grains when the angle  $\beta$  is larger than approximately  $72^\circ$ , while the  $(1\ 1\ 1)/[2\ \bar{1}\ \bar{1}]$  and  $(0\ 1\ 1)/[0\ 1\ \bar{1}]$  orientations become the most favorable at a lower  $\beta$  angle (less than  $72^\circ$ ). As indicated by the computational results, the  $(0\ 1\ 1)/[1\ 1\ \bar{1}]$  and  $(0\ 1\ 1)/[2\ \bar{1}\ 1]$  orientations have the largest maximum velocity ratios with a value of 1.73 and 1.63, respectively. Therefore, the susceptibility to stray grain formation is probably the highest in the melt-pool solidification for these asymmetric orientations.

Recently, Gaumann et al. [10] developed a more accurate microstructure criterion to avoid the columnar-to-equiaxed transition (CET) and thus the stray grain formation in single-crystal nickel-based superalloys through theoretical modeling. Current 3D melt-pool heat and fluid flow modeling techniques [11,12] can be used to obtain the melt-pool geometrical parameters defined in the present 3D melt-pool geometrical model and also to determine the temperature gradient as a function of position on the melt-pool solidification interface for a set of processing conditions. Applying the microstructure criterion established by Gaumann et al. to the 3D melt-pool geometry developed in this work by combining the distributions of temperature gradients and dendrite growth velocities in the melt pool, it is possible to predict the microstructure developments (columnar-dendritic and/to equiaxed-dendritic growth) and possibility of stray grain formation in the 3D melt-pool solidification of single-crystal alloys. Future work is to be conducted along this direction.

## 5. Conclusions

The mathematical model of the single-crystalline melt-pool solidification in LSM was used to compute the dendrite growth pattern and velocity distribution in the 3D melt pool under eight substrate orientation conditions. Results indicate that the substrate orientation has a predominant effect on crystal growth pattern and also influences the magnitude and distribution of the dendrite growth velocity in the single-crystalline melt-pool solidification. The selected  $\langle 1\ 0\ 0 \rangle$  growth variants and the number of chosen growth variants are dependent on the substrate orientation. Symmetric substrate orientations lead to symmetric microstructure patterns and symmetric velocity distributions, while non-symmetric orientations result in asymmetric microstructure patterns and asymmetric velocity distributions. The maximum ratio of dendrite growth velocity to the beam velocity in the melt pool is a function of melt-pool geometrical parameters and the substrate orientation.

The largest maximum velocity ratio for the symmetric orientations is 1.414 for the  $(0\ 0\ 1)/[1\ 1\ 0]$  and  $(0\ 1\ 1)/[0\ 1\ \bar{1}]$  orientations. The largest maximum velocity ratio for the asymmetric orientations is 1.732 for the  $(0\ 1\ 1)/[1\ 1\ \bar{1}]$  orientation. The analysis results show that the substrate orientation and melt-pool geometry have significant effects on the  $G/V$  ratio (temperature gradient over the growth velocity along the crystal growth direction) at the trailing point in the melt-pool solidification and thus influence the tendency to form stray grains in the melt pool. Experimental microstructure observations agreed well with the model predictions. These findings provide some important implications to practical applications in single-crystal surface processing.

## Acknowledgements

The authors gratefully acknowledge the financial support of this work by the National Science Foundation through a PECASE Award, Grant No. DMI 9983968, made through the Division of Manufacturing and Industrial Innovation of NSF. They thank Mr. S. Snider of Concorde Castings Inc. for providing the single-crystal alloys used in the experiments.

## References

- [1] Liu W, DuPont JN. Effects of melt pool geometry on crystal growth and microstructure development in laser surface-melted superalloy single crystals. Mathematical modeling of single crystal growth in a melt pool (Part I). *Acta Mater* 2004;52:4833–47.
- [2] Rappaz M, David SA, Vitek JM, Boatner LA. *Metall Trans A* 1989;20A:1125–38.
- [3] Rappaz M, David SA, Vitek JM, Boatner LA. *Metall Trans A* 1990;21A:1767–82.
- [4] Lancaster JF. *The physics of welding*. The International Institute of Welding (IIW). New York: Pergamon; 1984.
- [5] David SA, Vitek JM, Babu SS, Boatner LA, Reed RW. *Sci Technol Weld Joi* 1997;2:79–88.
- [6] Vitek JM, David SA, Boatner LA. *Sci Technol Weld Joi* 1997;2:109–18.
- [7] Park JW, Babu SS, Vitek JM, Kenik EA, David SA. *J Appl Phys* 2003;94(6):4203–9.
- [8] Fleming MC. *Solidification processing*. New York: McGraw-Hill; 1974.
- [9] Kurz W, Fisher DJ. *Fundamentals of solidification*. 3rd ed. Switzerland: Trans Tech Publications; 1989.
- [10] Gaumann M, Bezencon C, Canalis P, Kurz W. *Acta Mater* 2001;49:1051–62.
- [11] DebRoy T. In: David SA, Vitek JM, editors. *International trends in welding science and technology*. Materials Park, OH: ASM International; 1992. p. 17–25.
- [12] Weckman DC. In: Vitek JM, David SA, Johnson JA, Smartt HB, DebRoy T, editors. *Trends in welding research*. Materials Park, OH: ASM International; 1999. p. 3–12.